Rodríguez Martínez, ED.; Soriano Martinez, L.; Paya Bernabeu, JJ.; Borrachero Rosado, MV.; Monzó Balbuena, JM. (2012). Increase of the reactivity of densified silica fume by sonication treatment. Ultrasonics Sonochemistry. 19(5):1099-1107. doi:10.1016/j.ultsonch.2012.01.011.

# INCREASE OF THE REACTIVITY OF DENSIFIED SILICA FUME BY SONICATION TREATMENT

***Erich Rodríguez, Lourdes Soriano, Jordi Payá, María Victoria Borrachero, and, José M. Monzó*.***

errodnar@disca.upv.es, lousomar@upvnet.epv.es, jjpaya@cst.upv.es, vborrachero@cst.upv.es, jmmonzo@cst.upv.es. Instituto de Ciencia y Tecnología del Hormigón. Universitat Politècnica de València. Camino de Vera s/n, Edificio 4G, 46022 Valencia. Spain.

*Corresponding author: jmmonzo@cst.upv.es, phone +34 96 3877564.
Fax +34 963877569

## Abstract.

Five silica fumes from different manufacturers were subjected to ultrasonic treatment in order to decrease particle agglomeration and improve particle dispersion. The effectiveness of the sonication was observed as a reduction in particle size distribution of sonicated silica fume (SSF) compared to non-sonicated silica fume. SSF was added to Portland cement, which were analysed using thermogravimetric analyses (TGA/DTG) and scanning electron microscopy (SEM/EDX). The results were compared with those of control pastes made with untreated densified silica fume (DSF), as well as a reference cement paste of ordinary Portland cement (OPC). A maximum

grade of de-agglomeration by the sonication was obtained, with high volume of particles of diameter less than 1μm. Images obtained by transmission electron microscopy (TEM) of the SSF showed sintered particles that could be not fragmented by the treatment. Micro-structural characterisation results showed an increase in the reactivity of the silica fume after the treatment.

**Keywords:** Silica Fume; Particle size distribution; Dispersion; Thermal Analysis

## 1. Introduction

Silica fume is a very fine amorphous silica powder produced in electric arc furnaces as a by-product of the manufacture of alloys with silicon or elemental silicon. This silica fume by-product has been of significant interest to the concrete industry. Sharp (1) and Bernhard (2) were the pioneers in the field of silica fume in concrete and since the 1970s, the application of and interest in silica fume has increased. Today, silica fume is commonly used in the majority of industrial countries and also many developing countries. It is estimated that over 10 million cubic metres of concrete containing silica fume is cast every year (3). Due to its wide use, silica fume has been standardised by American (ASTM-C1240-10, CAN/CSA A23.5-98, NBR 13956-1997), European (EN 13263-2005), and Asian (GB/T18736-2002, JIS A 6207 2006, IS 15388:2003) standards.

The addition of silica fume to concrete mixes has both chemical and physical effects. The reactivity of silica fume is based on its high content of amorphous $SiO_2$ which reacts with the calcium hydroxide released during cement hydration via a pozzolanic reaction. Furthermore, silica fume is constituted of smaller particles than cement and can thus fill the spaces between cement grains leading to micro-filling or particle packing which contributes towards an increased compressive strength. Therefore, the use of silica fume as an admixture in concrete mixes has a positive effect on properties, such as: increased mechanical strength, low permeability, low shrinkage and increased chemical resistance amongst others (4, 5). However un-densified silica fume with particle size distribution smaller than 1 μm is rarely used as a mineral admixture in

concrete mixes due the difficulties of handling and transporting such a fine material. To overcome these problems, dry densified silica fume is frequently used. Densified silica fume is produced from silica fume by a densification process based on low heating and particle air flotation within a silo. The continuous motion of the individual spheres of silica fume promotes the creation of agglomerates. The material obtained consists of conglomerates of irregular shapes with sizes ranging between 10 μm to several hundred microns. This densified silica is not easily dispersed during the mixing of concrete and the agglomerates are not broken down completely (6-8). Ultra-fine spherical particles, smaller than cement grains, filling the gaps between cement particles improving the packing state, increasing the amount of free water, and the rolling effect due to the good shape of the particles. However, the use of densified silica fume has a negative effect on the workability of fresh mixes, where the rolling effect is lost due to the presence of agglomerates (9). Also un-reacted densified silica fume particles embedded into the hardened concrete might reduce its effectiveness to improve mechanical strength and permeability, where distinct reaction products replacing the silica within the boundary agglomerate has been observed. Furthermore, agglomerates of silica fume generating a calcium silicate hydrated (C-S-H) with a Ca/Si ratio very much less than the normal value in concrete (7, 10).

Dispersion of densified silica fume has previously been carried out by an alkali precipitation process in order to obtain silica nano-particles (11). However, ultrasound treatment applied to commercial densified silica fume is able to break and to disperse the agglomerates in order to obtain a more reactive material with a particle size

distribution lower than 1 μm, which can be used as a mineral admixture in concrete (12-14). The use of this sonicated silica fume as a mineral admixture in mortar mixes has a positive effect on the mechanical strength, where the compressive strength of mortars made with DSF obtained lower values. Longer sonication times and higher sonication power levels improved the effectiveness of silica fume through higher compressive strength as well as higher fixation of hydrated lime (12).

The reactivity and effectiveness of five silica fumes treated by a sonication process were evaluated in the present research. Portland cement pastes containing densified silica fume and sonicated silica fume were produced and analysed by thermogravimetric analysis (TGA/DTG) and scanning electron microscopy (SEM/EDS).

## 2. Experimental Procedure

### 2.1. Materials

Commercial densified (DSF) and non-densified (NDSF) silica fume from three different manufacturers and with different size distributions were used. Table 1 shows the chemical composition and physical properties of these materials.

As seen in figure 1A, DSF samples are made up of a great volume of large particles, which could be attributed to the micro-particles agglomeration, with sizes between 10 and 1000 μm. However, NDSF (figure 1B) had a lower average particle size. Less than 2% of particles were smaller than 1.0 μm (sub-micrometric particles) in DSF and NDSF. DSF-1 was finer, and had a wider particle size distribution than DSF-2 and

DSF-3. Although NDSF-1 and NDSF-2 are available commercially as non-densified materials, sub-micrometric particles were not observed, probably as a consequence of a agglomeration degree.

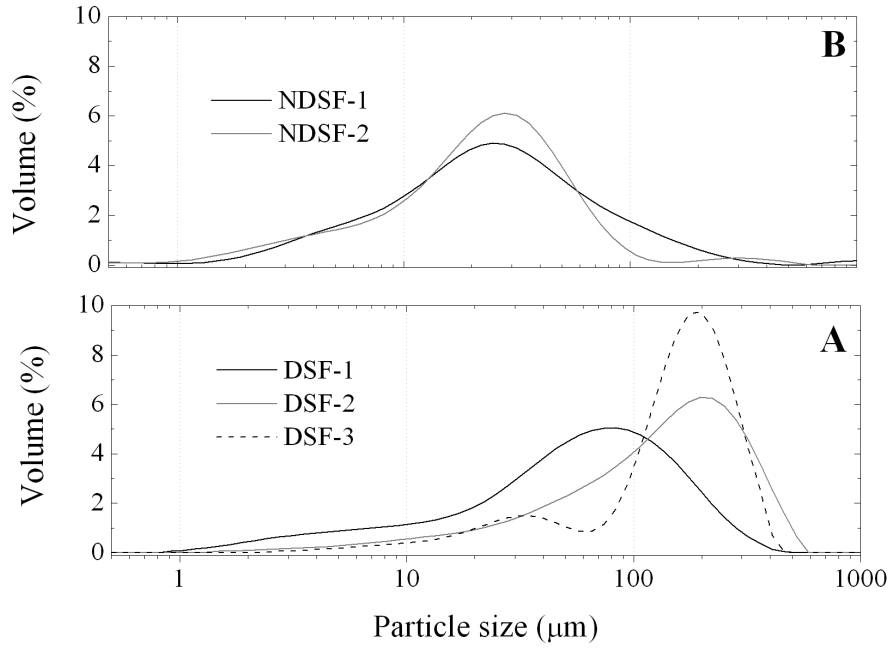


Figure 1 Particle size distribution of densified silica fumes (A) and non-densified silica fumes (B) determined by laser diffraction granulometer without any dispersing energy or flocculants agents.

Scanning electron microscopy images in figure 2, show large agglomerates of silica fumes particles (DSF-1, DSF-2, and DSF-3) with irregular shapes. It can also be seen

that, non-densified silica fume (NDSF-1), contains fewer agglomerates than densified materials, according to granulometric analysis.

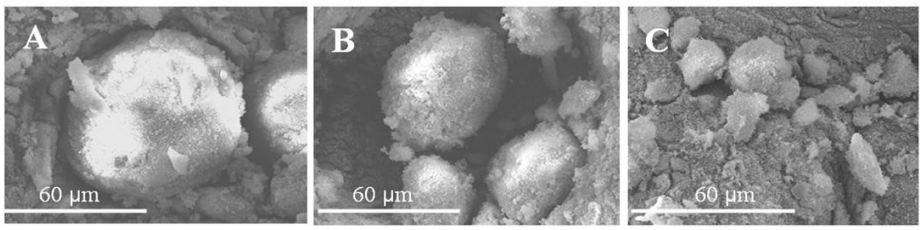


Figure 2 Scanning electron microscopy of densified and non-densified silica fume. A. DSF-1; B. DSF-3; C. NDSF-1

The materials evaluated mainly consisted of amorphous phases according to the XRD diffractograms shown in figure 3. However, traces of crystalline phases, such us quartz (Q) were identified in DSF-1 and DSF-2.

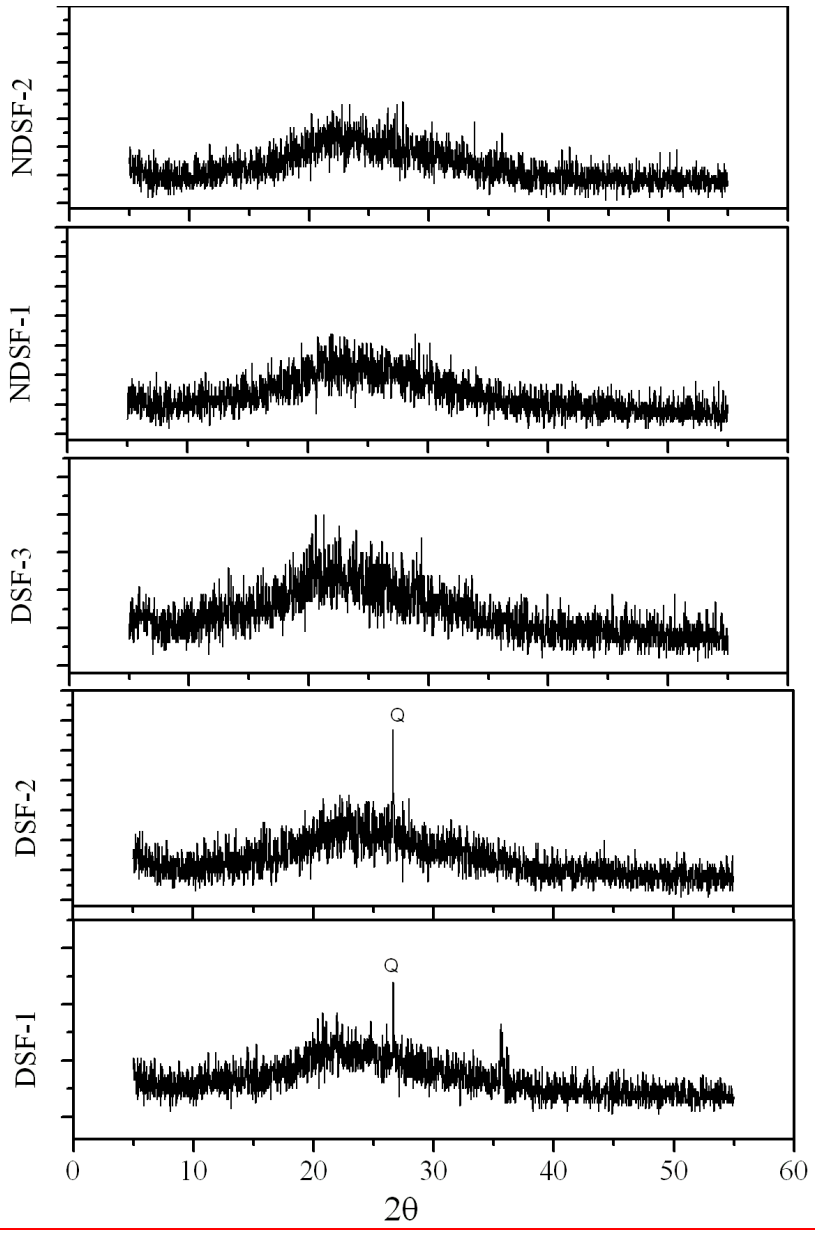


Figure 3 X-ray diffraction of densified and non-densified silica fumes.

### 2.2. Ultrasound treatment applied and sonicated sample production.

Ultrasonic treatments of each silica fume were carried out using a S-3000 sonicator from MISONIX. A maximum power of 600W with an output frequency of 20 kHz was applied. These values were chosen based upon the findings of previous research [8, 9]. Aqueous dispersions of 5g of silica fume and 20g of water were sonicated for 10 minutes. The increase in temperature of the suspension during the sonication treatment was controlled through use of an external cooling bath. The aqueous dispersion obtained after the treatment was mixed for three minutes with 45 g of cement CEM-I 52.5R (ASTM Type I). Chemical and physical properties of the used cement are shown in table 2. The pastes mixed with silica fume were produced with a water/binder ratio of 0.40 and 10% cement replacement. Pastes containing untreated densified and non-densified silica fume were prepared using the same dosages, in order to evaluate the effectiveness of the sonication. The fresh pastes were poured into hermetic plastic containers and stored in a chamber at 25 ºC and at a relative humidity of 90%. A paste of OPC without any mineral admixture was also produced as a reference sample.

### 2.3. Experimental techniques

The effect of the sonication treatment on particle sizes distribution was determined using laser diffraction analysis (LDA). Particle size measurements were carried out using a Master Sizer 2000 granulometer and analysed using Malvern Instruments software v3.01. Complementary, zeta potential were measured by electrophoresis apparatus through Malvern Instruments Zetasizer 2000. The sample used in zeta

potential test was previously diluted with distilled water. The suspension was injected into an electrophoresis cell and resulting data was an average of three measurements.

Densified silica fume (DSF) and sonicated silica fume (SSF) were characterized using transmission electron microscopy (TEM). One gram of the aqueous dispersion was diluted in 100 g of distilled water. A tiny drop was placed on a carbon grid and dried for a couple of hours at room temperature. The sample was analysed using a Philips SM10 and a maximum current of 100 kV.

Thermogravimetric analyses (TGA/DTG) were carried out in pastes cured for 1, 3, 7, 14 and 28 days. A TGA850 thermo-balance from Mettler Toledo and STARe® software v8.10 were used. Beforehand, the samples were milled, washed with acetone, filtered and then dried at 60 ± 2 ºC for approximately 30 minutes. For the TGA, aluminium crucibles of 100 µL were used and filled with 30±1 mg of dried sample. Samples were heated up to 600 ºC with a heating rate of 10 ºC/min in a nitrogen atmosphere

The microstructure of the samples after 28 days of curing was observed by scanning electron microscopy (SEM) in a JEOL JSM6300 from Oxford Instruments. The secondary electron images were obtained in samples coated with Au and using a current of 20 kV. Complementary cross section images and EDX130 analyses were obtained by backscatter electron mode SEM on a fragment of paste cured for 28 days and embedded in an epoxy resin.

## 3. Results and Discussion.

### 3.1. Sonication Treatments of densified and non-densified silica fumes

The shift of the particle sizes distribution as a consequence of the sonication treatment on densified silica fume (SSF samples obtained from DSF-1, DSF-2 and DSF-3) and non-densified silica fume (SNSF samples obtained from NDSF-1 and NDSF-2) is shown in figure 4. The volume of particles of smaller sizes was increased by the sonication treatment due to the dispersion of agglomerates. The mean particle size of SSF-1 after two and ten minutes was 7.83 μm and 2.41 μm, respectively. This treatment applied to DSF-1 reduced the mean particle size by a factor of 34, compared to the original untreated material. However, the sonication treatment was less effective for DSF-2 and DSF-3, where the shift in their particle size distribution during the first four minutes was considerably lower due to its superior agglomeration degree. The mean particle size was up to two times larger than that of SSF-1. However, no significant increase in the volume of sub-micrometer particles was observed, after longer treatment. On the other hand, a pronounced shift in the first two minutes for SNSF-1 was identified and no significant changes were observed with an increase in treatment time (figure 4B). Sonication treatment applied to SNSF-2 for ten minutes resulted in a consecutive process of de-agglomeration and agglomeration.

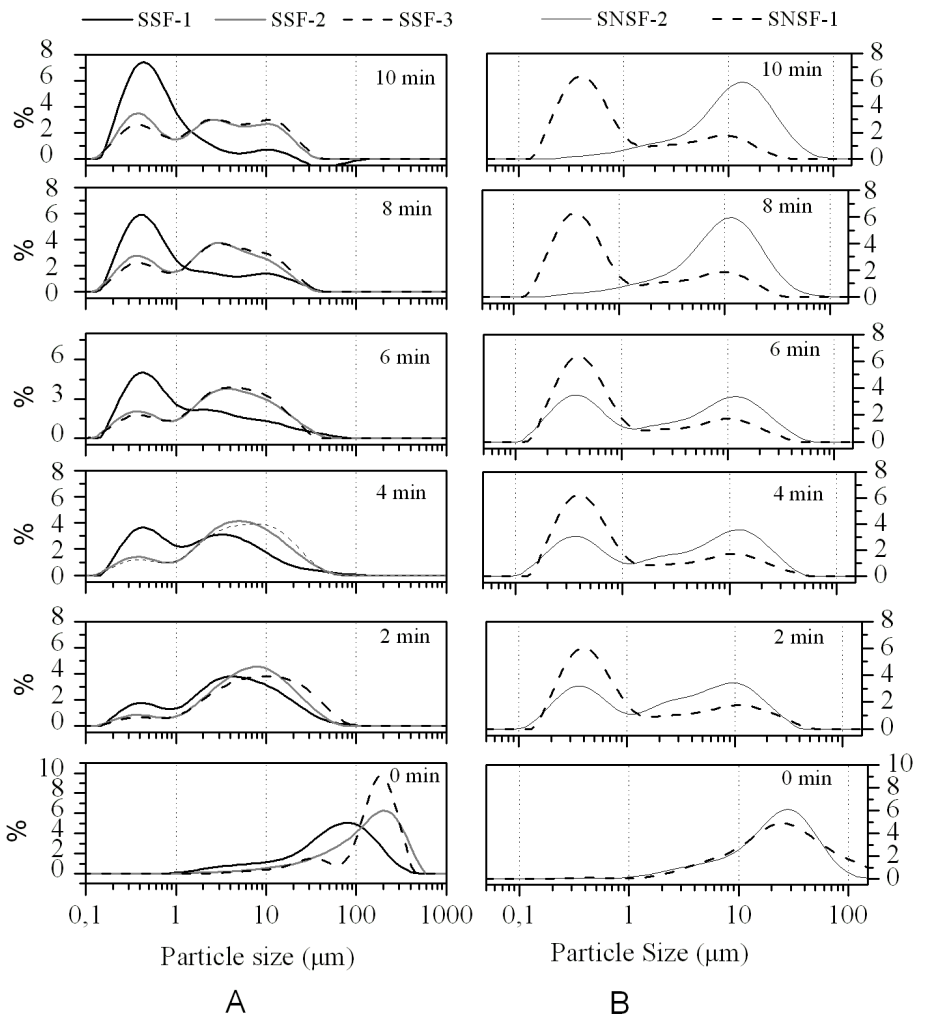


Figure 4 Effect of the sonication treatment on particle size distribution.

SSF samples; B. SNSF samples

Con formato: Normal

In accordance with the granulometric distribution of each material treated, percentiles 10, 50 and 90% (d(0,10); d(0,50), and d(0,90), respectively) were calculated and plotted in figure 5. Percentiles allow identification of the effectiveness of the treatment applied. DSF-1 exhibited a lower grade of agglomeration, showing that 50% of particles were of sizes smaller than 1.2 μm within only five minutes of treatment. Higher volumes of stronger agglomerates that were more difficult to break apart were identified in SSF-2 and SSF-3. Therefore, sonication treatment of DSF-2 and DSF-3 resulted in a decrease of the rate of particle size reduction with respect to that of DSF-1, as shown in figure 5. The values of d(0,50) for SNSF-1 sonicated from two to ten minutes were between 0.60 and 0.65 μm, and the d(0,10) value was 0.26 μm. Hence, a maximum grade of de-agglomeration of SNSF-1 is easy to obtain within a few minutes of sonication treatment. SNSF-2 reached its maximum grade of de-agglomeration after seven minutes of treatment; although treatment for longer time periods resulted in re-agglomeration. High increases in values of percentiles from seven to ten minutes of treatment were observed.

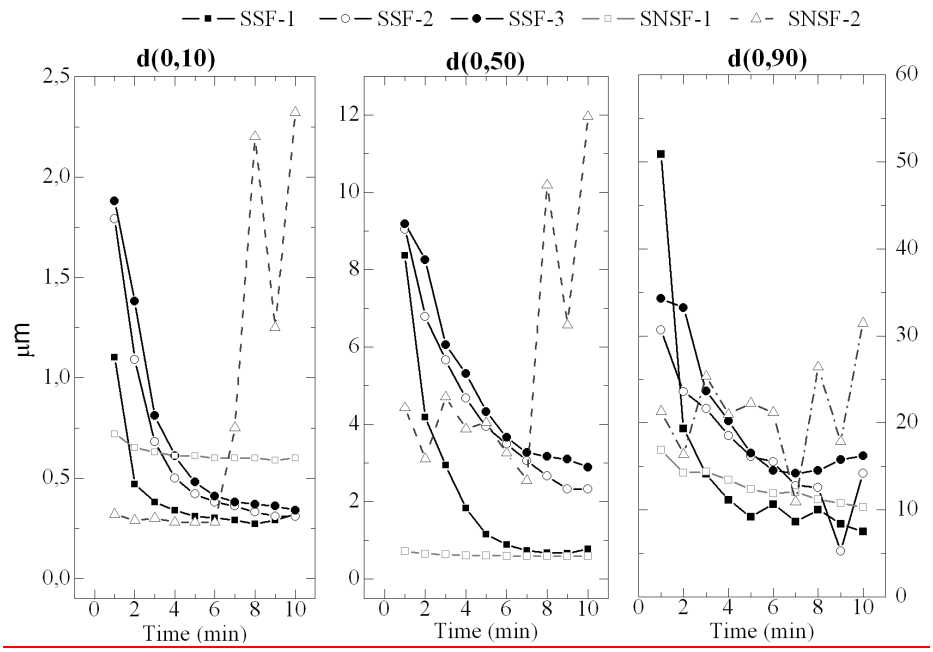


Figure 5 Percentiles d(0,10); d(0,50) and d(0,90) from particle size distributions of SSF and SNSF

Figure 6 shows the volume of sub-micrometric particles (particles with diameter lower than 1µm) obtained during the treatment for each sample and treatment time. SSF-2 and SSF-3 exhibited a linear increase in the volume of sub-micrometric particles with sonication time. The highest volume of sub-micrometric particles obtained for SSF-2 and SSF-3 was 36.2% and 29.8%, respectively. These values were achieved after 10 minutes of treatment. The maximum de-agglomeration of SSF-1 and SNSF-1 which occurred during eight minutes and two minutes of treatment respectively was determined by analysis of the content of sub-micrometric particles, which was

approximately in the range of 65% to 62%. A decrease in sub-micrometric particle content and an agglomeration process was observed for SNSF-2. A 35% -39% sub-micrometric volumes of particles for SNSF-2 was obtained when treatment was applied for two to six minutes. However, on further increasing the treatment time to ten minutes resulted in a 3.5% reduction in sub-micrometric particle volume. This behaviour might be attributed to a reduction in electrostatic forces, which promotes the particle agglomeration and reduces dispersion.

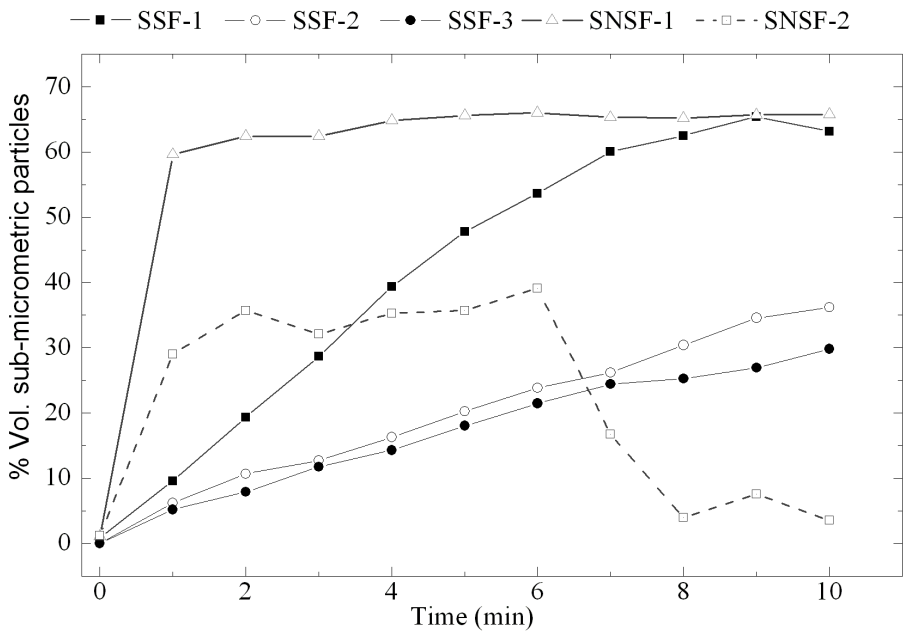


Figure 6 Effect of sonication time on the volume of sub-micrometric particles

Zeta potential is a property related to the electrical potential around a particle on the slip surface within a double layer formed in the stationary layer of fluid attached to the

dispersed particle (15). The liquid layer surrounding the particle is constituted in two sections: the stern layer where the ions are strongly bounded to the particle and an outer or diffusive layer where they are less strongly attached. Zeta potential is an indicator of the stability of a colloidal system. If the suspension has a large negative or positive zeta potential, particles will tend to repel each other and there will be no tendency for the particles to come together or to agglomerate. However, if the particles have low zeta potential values there will be no force to prevent the particles coming together. Table 3 shows the zeta potential measured for SSF-1, SNSF-1, SSF-2, and SNSF-2 suspensions after 2 and 8 minutes sonication. The values presented are an average of three measurements from an individual sonicated suspension. The values of Zeta potential obtained are in coherence with the grade of particles dispersion (figure 4 and figure 6), as well as the effectiveness of the treatment. The highest zeta potential value obtained was of -31.3 mV for the suspension SNSF-1 after 2 minutes of sonication, which corresponds to the highest grade of deagglomeration with the lower time of treatment. A slight reduction of zeta potential was observed after sonication for 8 minutes. The effectiveness of the treatment is again identified by the zeta potential, where SSF-2 with 8 minutes has a zeta potential two times lower than that of SSF-1 showing a relation between the content of sub-micrometric particles and particle size distribution, due to the fact that electrophoretic mobility is only dependent on the particle size and shape, as well as the properties of the electrolyte solution in which they are dispersed (16, 17). Therefore the lower value of zeta potential in SSF-2 is related to the lower content of sub-micrometric particles and its low stability. Likewise, increasing sonication time from 2 to 8 minutes for SSF-1 and SSF-2 has a positive effect on zeta potential, such

that after 8 minutes of treatment, the zeta potential is up to 71% higher and the suspension starts to become more stable.

Figure 7 shows the TEM images of the original untreated DSF-1 (fig. A) and the corresponding sonicated sample of SSF-1 (fig. B and C). Agglomerates of 23μm in size with an irregular shape and comprised of thousands of microspheres of silica fume can be seen in figure 7A. The energy applied by the sonication breaks the weak bond between individual silica fume particles (figure 7B). The mean diameter measured by image analysis of the individual silica fume sphere particles via TEM was ~80 nm. The particles obtained after the densification process during silica fume manufacture are made up of a huge volume of agglomerated particles, held together by Van der Waals forces and are designed to break easily during handling and mixing. However, during the manufacture process, the surface of the silica fume particles might melt and being in direct contact with other particle, many hundreds of such particles can solidify together to create new aggregates, where the formation of aggregates during condensation depends on the particle concentration in the gas volume as well as the off-gas temperature. This phenomenon is a frequent occurrence and creates bonds that are a lot stronger than those of Van der Waals that are not so easy to break via traditional mixing processes (18) . Figure 7D shows particles sintered exhibit solid material bridges that cannot be dispersed or fragmented by sonication treatment. These types of sintered particles could be the responsible for limiting the maximum content of sub-micrometric particles obtained after the sonication treatment, so that complete deagglomeration/dispersion cannot be achieved. Increasing the energy applied to DSF

through longer sonication treatments, did not lead to further dispersion. Therefore, a distinction between agglomerates and aggregates of silica fume might be identified, where the strength of interparticle bonds determines the product properties, and the energy needed for particle de-agglomeration could be considerably different.

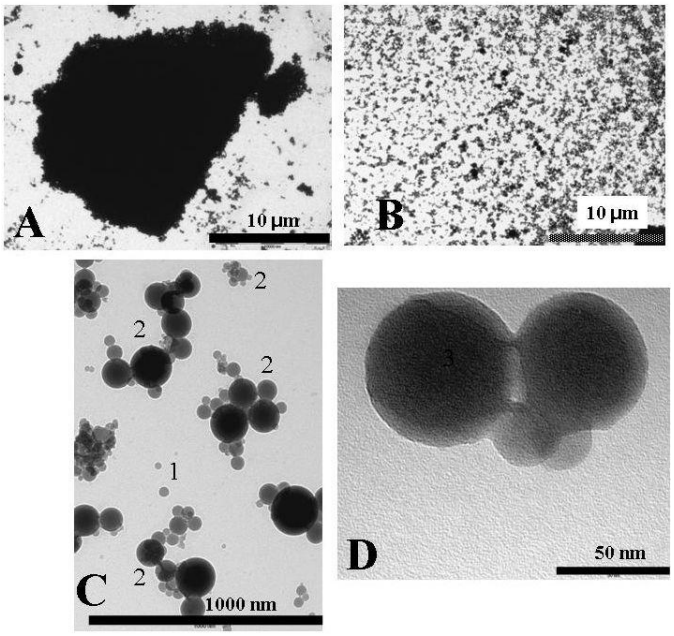


(1) Individual Silica Fume Particles; (2) Agglomerate/aggregate of silica fume particles

Figure 7 Transmission electron microscopy (TEM) images obtained from original DSF-1 and SSF-1. A. Silica Fume agglomerate; B. Agglomerate of silica fume fragmented by the sonication treatment; C. Sonicated silica fume particles; D. Nanoparticles of silica fume sintered

### 3.2. Microstructural characterization of pastes containing silica fume

Thermogravimetric results (TG curves) of the reference paste (OPC), pastes with sonicated silica fume (SSF) and pastes with untreated densified silica fume (DSF) are shown in figure 8. Derivative curves DTG (dashed lines) show two relevant mass loss events in the ranges 35ºC - 200ºC, and 500ºC - 600 ºC. The first stage corresponds to the $H_2O$ released from the hydrated phases, such as ettringite ($C_6AS_3H_{32}$), hydrated calcium silicates (C-S-H), and calcium aluminosilicate hydrates (CASH, $C_2ASH_8$). Second stage is attributed to the dehydroxylation of portlandite (CH). Based on TG data from each paste of SSF and DSF with different age of curing, dehydration of Portlandite as a consequence of a mass loss between 500º and 600ºC were calculated according to Payá *et al.* (19) Therefore, the percentage of portlandite, of $H_2O$ combined with the reaction products (except portlandite), and of portlandite fixed by pozzolanic reaction were calculated according to equation 1, 2 and 3, respectively.

$$\%H_2Ocombined = LW^t_{Total} - LW^t_{CH} \qquad Ec1$$

$$\%CH = LW_{CH} \cdot \left( \frac{PM_{CH}}{PM_{H_2O}} \right) \qquad Ec2$$

$$\%Fixed\ Portlandite = \left( \frac{(CH_C \cdot C) - CH_P}{CH_C \cdot C} \right) \cdot 100 \quad Ec3$$

Where:

$LW_{Total}^t$ is the total mass loss obtained by heating from temperatures between 35º and 600ºC after curing for time ‘t’.

$LW_{CH}^t$ is the mass loss related with the dehydration of portlandite occurring at temperatures between 500º and 600 ºC after curing for time ‘t’.

$PM_{CH}$ y $PM_{H2O}$ are the molecular weight of portlandite and water, respectively.

$CH_C$ is the Portlandite content in the reference material (OPC paste).

$CH_P$ is the Portlandite content in the paste with DSF or SSF.

C is the cement proportion in the binder, in this research 0.90.

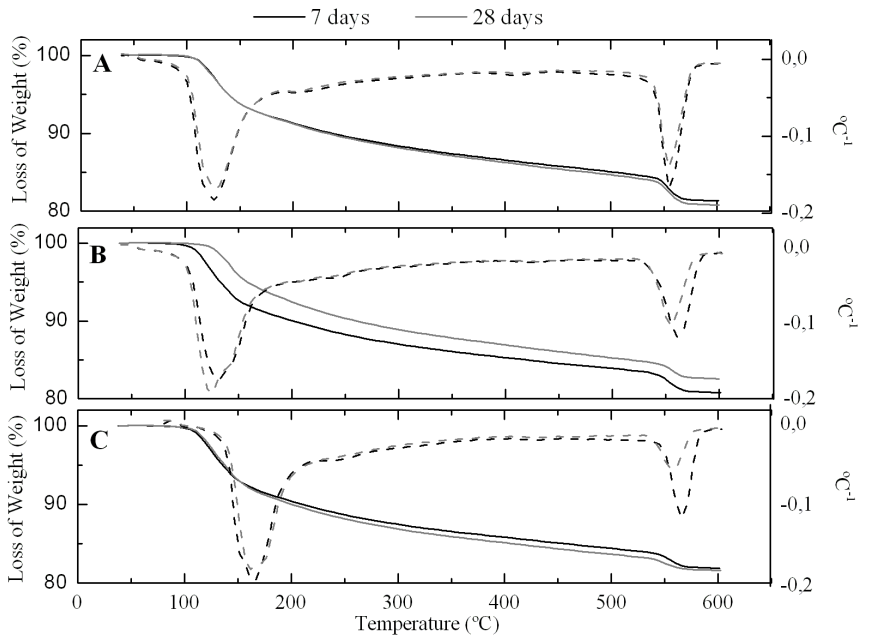


Figure 8 Thermogravimetric analysis curves (TG left axis; and DTG right axis) for pastes with 7 and 28 days of curing. A. OPC; B. DSF-1, and C. SSF-1.

Table 4 shows the $\%H_2O_{combined}$, %CH, and % Fixed Portlandite present in the reference material paste, as well as for pastes containing untreated silica fume and sonicated silica fume. In general, for all SF pastes a decrease in CH was observed with an increase in curing age. Likewise, the sonication treatment applied to densified and non-densified

silica fumes enhanced the reactivity of both, due to an increase in fixed portlandite values compared with the untreated silica fume pastes. At early ages of curing (one day), negative values of fixed portlandite were observed in some sonicated and non-sonicated SF pastes. In some cases, the use of silica fume accelerated the hydration of cement tricalcium silicate. This may have been due to silica fume particles initiating the nucleation of hydrated products from Portland cement. Several researchers (20, 21), have shown that ultrafine particles of inert (for example $Al_2O_3$) or active filler (for example SF) can accelerate the initial hydration reaction. Agglomerates of silica fume particles adsorb free water available for cement hydration resulting in less water contributing to the hydration process (21). Pozzolanic reaction occurs with the increasing of the age of curing, as the silica fume promotes the precipitation of C-S-H, allowing the fixation of portlandite. DSF-3 showed the lowest pozzolanic reactivity in comparison to the other mineral admixtures. Portlandite fixed after 7 days of curing had a value of 13.2%, significantly lower than those values obtained for DSF-1 and DSF-2, under the same conditions. Moreover, it is clear after comparing with paste samples of DSF and NDSF that CH content can be reduced when SSF or SNSF is used. CH content is further reduced when SSF-1 is added, presenting the highest reactivity with a fixed portlandite up to 61.2% after 28 days. Although, the phases detected using TGA were similar to those of DSF and SSF, it was noticed from DTG analyses that there was a decrease in the content of CH with the use of SSF or SNSF compared to DSF or NDSF. This behaviour was due to the increased pozzolanic activity that can occur when silica fume is sonicated. Therefore, more C-S-H can be detected in sonicated pastes (SSF and SNSF). This was identified by a slight increase in $H_2O$ released from hydrates phases

when compared to pastes with non-treated silica fume (DSF and NDSF) at the same curing age.

Figure 9 shows the effectiveness of the sonication treatment on the reactivity of densified silica fumes. The relation between the CH fixed in the pastes with densified (DSF) or sonicated silica fume (SSF) was calculated by equation 4, where $CH_{SSF}$ and $CH_{DSF}$ are the mass losses attributed to CH for the sonicated and densified silica fume pastes, respectively.

$$\text{Re}\,duction\ of\ the\ content\ of\ Ca(OH)_2 = \left(\frac{CH_{HSS} - CH_{HSD}}{CH_{HSD}}\right)\cdot 100 \quad \text{Eq. 4}$$

The pastes produced with sonicated silica fume present up to 44% lower CH content than that of the pastes containing untreated silica fume. The sonication treatment notably increases the reactivity of the silica fume regardless of the grade of densification of the starting material. Sonicated silica fume used as a mineral admixture in Portland cement systems, has a higher pozzolanic activity caused by its increased ability to react with portlandite released from the cement hydration. At early ages of curing, the reactivity of SSF-2 and SSF-3 is 14% higher than that of the original materials without treatment (DSF-2 and DSF-3). In addition, the ability of sonicated silica fumes to react with CH increases with curing age. Pastes with SSF-1, SSF-2, and SSF-3 after 28 days of curing showed a 36%, 34%, and 43% reduction in portlandite compared to pastes with densified silica fume (DSF-1, DSF-2, and DSF-3, respectively).

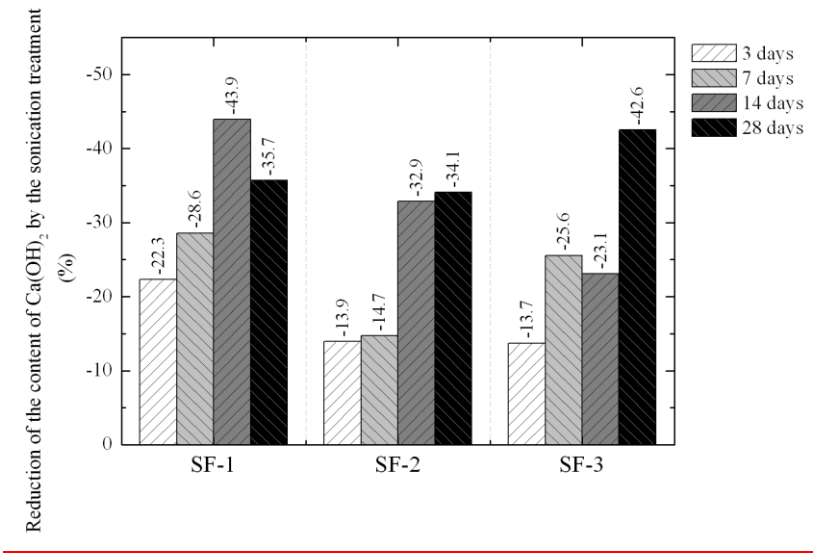


Figure 9 Effectiveness of the sonication treatment for densified silica fumes

The microstructures of pastes produced with SSF-1 and DSF-1 after 28 days of curing were analysed using SEM/EDS. Figure 10A shows a SEM micrograph of the DSF-1 paste and identifies an un-reacted densified silica fume particle. The un-reacted agglomerate is over 70 μm in size. Un-dispersed silica fume agglomerates present in concrete have been reported by other authors (22, 23). Alkali-silica reaction (ASR) in silica fume aggregates has been also identified. However, this type of ASR detected in concrete does not cause significant deterioration (7). The backscattered SEM image from figure 10B shows the cross section of un-reacted silica fume agglomerate with a diameter larger than 80 μm.. However, a partial bond between silica fume agglomerate and paste is observed in the backscattered image (indicated by an arrow in the fig. 10B). EDX analysis of the interface of DSF-1 agglomerate and hydrated paste of cement

shows a decrease in calcium content from the hydrated paste to the centre of the particle. A lineal EDX examination (white line in figure 10B) shows a various compounds formed around interface during cement hydration, which presents a different content of calcium and silica. At the border of the DSF agglomerate an atomic Ca/Si ratio of 0.48 was identified (square 2 in figure 10B) and might be attributed to the presence of CH, as well as only a portion of C-S-H. However in the hydrated paste, this atomic Ca/Si ratio was higher (2.80 according with EDX data in square 1 in figure 10B). Therefore, in the paste containing DSF-1, the formation of CSH due to the pozzolanic reaction was concentrated around the agglomerates and the C-S-H content in the hydrated paste was lower.

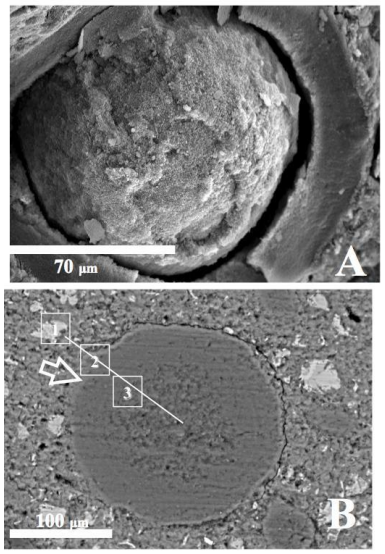


**1.**

| Element | Weight% | Atomic% | Compd% | Formula |
|---|---|---|---|---|
| Al K | 1.83 | 1.67 | 3.45 | $Al_2O_3$ |
| Si K | 11.23 | 9.86 | 24.03 | $SiO_2$ |
| Ca K | 44.91 | 27.63 | 62.84 | CaO |
| Fe K | 1.21 | 0.53 | 1.55 | FeO |
| O | 37.22 | 57.36 | | |
| Ca/Si Ratio | 4.0 | 2.80 | 2.62 | |

**2.**

| Element | Weight% | Atomic% | Compd% | Formula |
|---|---|---|---|---|
| Al K | 0.31 | 0.25 | 0.58 | $Al_2O_3$ |
| Si K | 31.56 | 24.76 | 67.51 | $SiO_2$ |
| Ca K | 21.80 | 11.98 | 30.50 | CaO |
| O | 45.25 | 62.32 | | |
| Ca/Si Ratio | 0.69 | 0.48 | 0.45 | |

**3.**

| Element | Weight% | Atomic% | Compd% | Formula |
|---|---|---|---|---|
| Si K | 38.40 | 28.85 | 82.15 | $SiO_2$ |
| Ca K | 10.42 | 5.49 | 14.58 | CaO |
| O | 48.60 | 64.10 | | |
| Ca/Si Ratio | 0.27 | 0.19 | 0.18 | |

Figure 10 Scanning electron microscopy (SEM) of pastes with original DSF-1 without treatment.

Figures 11A and B show the SEM images of the paste produced using SSF-1, where individual silica fume particles of diameter less than 2 μm were observed (see white arrows in figure 11A). A homogeneous microstructure without the presence of large silica fume agglomerates was identified in the backscattering images of the cross section. The atomic Ca/Si ratio in the hydrated paste is in the range 1.64 - 1.83 which can be attributed to C-S-H phases, values considerably lower than that obtained for corresponding pastes containing DSF-1. This could be attributed to a more homogeneous dispersion of the silica particles of SSF-1, which contributes to C-S-H formation. Therefore an increase in the reactivity of DSF as a result of sonication treatment agrees with SEM/EDS images.

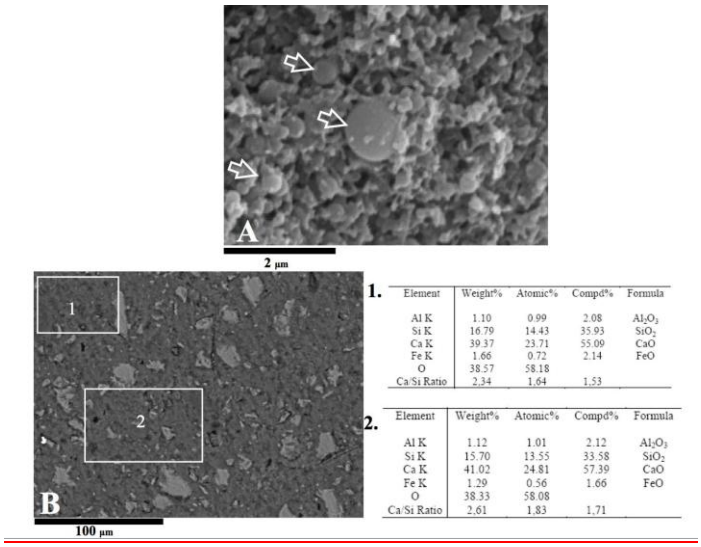


1.

| Element | Weight% | Atomic% | Compd% | Formula |
|---|---|---|---|---|
| Al K | 1.10 | 0.99 | 2.08 | $Al_2O_3$ |
| Si K | 16.79 | 14.43 | 35.93 | $SiO_2$ |
| Ca K | 39.37 | 23.71 | 55.09 | CaO |
| Fe K | 1.66 | 0.72 | 2.14 | FeO |
| O | 38.57 | 58.18 | | |
| Ca/Si Ratio | 2.34 | 1.64 | 1.53 | |

2.

| Element | Weight% | Atomic% | Compd% | Formula |
|---|---|---|---|---|
| Al K | 1.12 | 1.01 | 2.12 | $Al_2O_3$ |
| Si K | 15.70 | 13.55 | 33.58 | $SiO_2$ |
| Ca K | 41.02 | 24.81 | 57.39 | CaO |
| Fe K | 1.29 | 0.56 | 1.66 | FeO |
| O | 38.33 | 58.08 | | |
| Ca/Si Ratio | 2.61 | 1.83 | 1.71 | |

Figure 11 Scanning electron microscopy (SEM) of pastes with sonicated silica fume (SSF-1).

## 4. Conclusions

The sonication treatment applied to densified silica fume contributes with the increasing of its reactivity by a de-glomeration mechanism. The treatment breaks up the agglomerates as well as improving dispersion. However the effectiveness of the treatment is related to the grade of densification of silica fume (which contained sintered together micro-silica particles). Silica fume particles were uniformly dispersed into cement paste, increasing its reactivity in order to react with calcium hydroxide from hydrated paste to form C-S-H phases. An important decrease in calcium hydroxide content, after 28 days of curing, was observed when cement pastes were prepared using sonicated silica fume (SSF) samples.

## 5. Acknowledgments

Acknowledgments to Ministerio de Ciencia e Innovación (Project BIA-2007-63252 and research scholarship BES-2008-002440) of Spain, European regional development fund (FEDER), and Ferroatlantica S.L. for the support on the development of this research. A special acknowledgement is also due to the Centre of Electron Microscopy of the Universitat Politècnica de València

## 6. References

1. J.W. Sharp. Silica Modified Cement. United State Patent Office. Patented Nov. 12. 1946. 2,410,954.

2. C.J. Bernhard. SiO2-støv som cementtilsetning. Betongen Idag. Organ for Norsk Cementforening. NR2. Arpil 1952.
3. P. Fidjestol and M. Dastol. The History of Silica Fume in Concrete. *Ibracon* (Congresso Brasilero do Concreto) 50CBC. Sao Paulo. Brazil (2008).
4. D. D. L.. Chung, . Improving cement-based materials, J. Mater. Sc. 37 (2002) 673 - 682.
5. E. A. Kishar, D. A. Ahmed, and M. R. Mohammed, Hydration of Portland cement in presence of silica fume. Adv. Cem. Res. 22:3 (2010) 143-148.
6. D. Baweja, T. Cao, and L. Bucea. Investigation of dispersion levels of silica fume in pastes, mortars, and concrete, in: Proceedings of CANMET/ ACI Conference on Concrete Durability, Athens, ACI SP 212, American Concrete Institute, Farmington Hills, MI, USA, 2003 1019–1034.
7. S. Diamond, S. Sahu, and N. Thaulow, Reaction products of densified silica fume agglomerates in concrete, Cem. Concr. Res. 34 (2004) 1622-1632.
8. D. R. G.Mitchell, I. Hinczak, and and R. A. Day. Interaction of silica fume with calcium hydroxide solutions and hydrated cement pastes. Cem. Concr. Res., 28:11 (1998) 1571-1584.
9. Sakai, E., Kakinuma, Y., Yamamoto, K., & Daimon, M.. Relation between the Shape of Silica Fume and the Fluidity of Cement Paste at Low Water to Powder Ratio. J. Adv. Concr. Technol 7:1 (2009) 13-20.
10. A. Shayan. Morphological, mineralogical and chemical features of steam-cured concretes containing densified silica fume and various alkali levels. Adv Cem. Res. 5:20 (1993) 151-162.
11. M. M. Rashad, M. M. Hessien, E. Abdel-Aal, K. El-Barawy, and R. K. Singh.. Transformation of silica fume into chemical mechanical polishing (CMP) nano-slurries for advanced semiconductor manufacturing. Powder Technol. , 205:1-3 (2011) 149-154.
12. G. M. Gapinski and J. Scanlon. Silica fume. Norchem. (2005) doi: 10.1016/S0008-8846(97)00191-9.

13. D. Martinez, J. Payá, J.M. Monzó, and M.V. Borrachero . Granulometric activation of densified silica fume (CSF) by sonication, Adv. Cem. Res. 20:3 (2008) 129-135.
14. D. Martinez, J. Payá, J.M. Monzó, and M.V. Borrachero V., Effect of Sonication on the reactivity of Silica Fume in Portland Cement Mortars, Adv. Cem. Res. 23:1 (2011) 23-31.
15. S. Srinivasan, S. Barbhuiya, D. Charan, and S. P. Pandey. (2010). Characterising cement–superplasticiser interaction using zeta potential measurements. Constr. Build. Mater. 24:12 (2010) 2517-2521.
16. R. W.O'Brien, L. R. White, Electrophoretic Mobility of Spherical Colloidal Particle, J. Chem. Soc. Farad. T. 2 74
17. P. H. Wiserma, A. L. Loeb, and J. T. G.Overbeek, J. T. Calculation of Electrophoretic Mobility of a Spherical Colloid Particle. J. Colloid. Interface Sci. 22:78 (1699).
18. M. Seopenbusch, S. Rothenbacher, M. Kirchholf, H.J. Schmid, G. Kasper, and A.P. Weber, Interparticle forces in Silica nanoparticle agglomerates, J. Nanopart. Res. 12 (2010) 2037-2044.
19. J. Payá, J.M. Monzó, M.V. Borrachero, and S. Velazquez. Evaluation of Poozolanic Activity of Fluid Catalytic Cracking Residue (FC3R). Thermogravimetric Analysis studies on FC3R-Portalnd. Cement Pastes. Cem. Concr. Res. 33 (2003). 603-609.
20. W. A. Gutteridge and J. A. Dalziel. (1990). Filler cement the effect of the secondary component on the hydration of Portland cement. Cemen. Concr. Res. 20 (1990) 778-782.
21. E.H. Kadri and R. Duval, Hydration heat kinetics of concrete with silica fume, Constr. Build. Mater. 23 (2009) 3388-3392.
22 J. Yajun and J.H. Cahyadi, Effects of densified silica fume on microstructure and compressive strength of blended cement pastes, Cem. Concr. Res. 33 (2003) 1543-1548.
23. D. Bonen and S. Diamond, Occurrence 1 of large silica fume-derived particles in hydrated cement paste, Cem. Concr. Res. 22 (6) (1992) 1059-1066.

1 Table 1 Chemical Composition of commercial silica fume samples.

| | DSF-1 | DSF-2 | DSF-3 | NDSF-1 | NDSF-2 |
|---|---|---|---|---|---|
| $SiO_2$ | 95.8 | 90.77 | 95.51 | 96.30 | 88.75 |
| $Al_2O_3$ | 0.31 | 0.46 | 0.44 | 1.05 | 0.47 |
| $Fe_2O_3$ | 0.14 | 4.56 | 0.08 | 0.16 | 5.90 |
| CaO | 0.38 | 0.78 | 0.70 | 0.38 | 0.81 |
| MgO | 0.10 | 0.23 | 0.23 | 0.43 | 0.24 |
| $SO_3$ | 0.02 | 0.02 | 0.01 | 0.18 | 0.02 |
| $K_2O$ | 0.24 | 0.37 | 0.41 | 1.09 | 0.41 |
| $Na_2O$ | 0.08 | 0.21 | 0.11 | 0.20 | 0.23 |
| LOI (950ºC) | 3.85 | 3.43 | 3.15 | 2.10 | 4.03 |
| Mean particle size D[4,3] (μm) | 82.5 | 170.2 | 174.8 | 56.5 | 35.0 |
| Specific surface* ($m^2$/kg) | 152.0 | 27.0 | 41.8 | 281.0 | 328.0 |
| Specific weight (kg/$m^3$) | 2230 | 2260 | 2250 | 2270 | 2260 |

2 *Determined by Laser diffraction analysis software.

3

1 Table 2 Chemical and physical properties of cement (CEM-I 52.5R)

| | | |
|---|---|---|
| Chemical Composition | $SiO_2$ | 19.9 |
| | $Al_2O_3$ | 5.38 |
| | $Fe_2O_3$ | 3.62 |
| | CaO | 63.69 |
| | MgO | 2.14 |
| | $SO_3$ | 3.66 |
| | $K_2O$ | 1.17 |
| | $Na_2O$ | 0.10 |
| | PF | 2.02 |
| | RI | 0.95 |
| Physical features | Specific Weight ($kg/m^3$) | 3140 |
| | Mean particle diameter (μm) | 15.01 |

2

3

Table 3 Zeta Potential and conductivity of suspensions sonicated for 2 and 8 minutes.

| | Zeta Potential (mV) | | Conductivity (mS/cm) | |
|---|---|---|---|---|
| Time of Sonication | 2 min | 8 min | 2 min | 8 min |
| SSF-1 | -16.2 | -27.8 | 0.155 | 0.156 |
| SNSF-1 | -31.3 | -27.6 | 0.154 | 0.156 |
| SSF-2 | -11.6 | -15.0 | 0.156 | 0.156 |
| SNSF-2 | -25.7 | -24.3 | 0.160 | 0.155 |

Table 4. Total mass loss from combined water in pastes with original silica fume without treatment (DSF and NDSF), silica fume subjected to the sonication treatment (SSF and SNSF), and paste reference without mineral admixture (OPC).

| | $H_2O$ released from the hydrated phases | | | | | Fixed Portlandite evolution ($Ca(OH)_2$) | | | | |
|---|---|---|---|---|---|---|---|---|---|---|
| | Age of curing (days) | | | | | Age of curing (days) | | | | |
| | 1 | 3 | 7 | 14 | 28 | 1 | 3 | 7 | 14 | 28 |
| OPC | 12.9 | 15.5 | 16.1 | 15.5 | 16.5 | -- | -- | -- | -- | -- |
| DSF-1 | 11.9 | 15.5 | 17.2 | 16.3 | 16.1 | -4.1 | 4.5 | 10.3 | 4.6 | 39.7 |
| SSF-1 | 12.7 | 16.2 | 16.6 | 16.2 | 17.5 | 3.5 | 25.8 | 35.9 | 46.5 | 61.2 |
| DSF-2 | 12.9 | 16.8 | 14.2 | 15.2 | 15.5 | 4.2 | 9.5 | 19.9 | 9.5 | 24.9 |
| SSF-2 | 16.2 | 17.2 | 14.8 | 15.3 | 15.9 | -7.4 | 22.1 | 31 | 39.3 | 50.5 |
| DSF-3 | 13.6 | 13.8 | 14.9 | 12.4 | 19.8 | -9.0 | 4.7 | 13.2 | 10.4 | 8.5 |
| SSF-3 | 11.9 | 13.7 | 14.8 | 18.4 | 17.8 | -3.2 | 17.8 | 35.4 | 31.1 | 47.5 |
| NDSF-1 | 12.1 | 13.6 | 15.1 | 18.5 | 19.4 | 14.2 | 25.6 | 38.8 | 31.2 | 42.3 |
| SNSF-1 | 11.4 | 15.0 | 17.0 | 15.2 | 19.9 | 9.3 | 16.1 | 34.8 | 36.0 | 48.6 |
| NDSF-2 | 12.6 | 17.7 | 16.3 | 15.2 | 15.7 | -13.2 | 4.8 | 23.3 | 11.2 | 25.8 |
| SNSF-2 | 14.4 | 13.6 | 14.8 | 15.3 | 20.0 | -3.8 | 25.9 | 30.3 | 39.3 | 49.9 |